Techniques in Coloproctology (2025) 29:20
https://doi.org/10.1007/s10151-024-03056-5

ORIGINAL ARTICLE

Deep learning for segmentation of colorectal carcinomas on endoscopic ultrasound

F. van den Noort[1] · F. ter Borg[2] · A. Guitink[2] · J. Faber[3] · J. M. Wolterink[1]

Received: 23 April 2024 / Accepted: 6 November 2024

Abstract

Background Bowel-preserving local resection of early rectal cancer is less successful if the tumor infiltrates the muscularis propria as opposed to submucosal infiltration only. Magnetic resonance imaging currently lacks the spatial resolution to provide a reliable estimation of the infiltration depth. Endoscopic ultrasound (EUS) has better resolution, but its interpretation is investigator dependent. We hypothesize that automated image segmentation of EUS could be a way to standardize EUS interpretation.

Methods EUS media and outcome data were collected prospectively. Based on 373 expert manual segmentations, a convolutional neural network was developed to perform segmentation of the submucosa, muscularis propria, and tumors. The mean surface distance (MSD), maximal distance between segmentations (Hausdorff distance; HDD), and overlap (Dice similarity index; DSI) were calculated.

Results The median MSD and HDD values were 3.2 and 17.7 pixels for the tumor, 3.4 and 24.7 pixels for the submucosa, and 2.6 and 20.0 pixels for the muscularis propria, respectively. The median DSI values for the tumor, submucosa, and muscularis propria were 0.82, 0.57, and 0.59, respectively. These values reflect good agreement between manual and deep learning segmentation.

Conclusions This study found encouraging results of using automated analysis of EUS images of early rectal cancer, supporting further exploration in clinical practice.

Keywords Rectal cancer · Diagnostic imaging · Endosonography · Deep learning

Introduction

Since the introduction of population-based immunological fecal occult blood screening, the discovery of suspected polyps or early rectal cancer (SPEC) has increased [1]. SPECs are candidates for endoscopic submucosal dissection (ESD) or endoscopic intramural dissection (EID), in which the lesion is dissected from the muscularis propria or the longitudinal muscular layer of the rectal wall. However, in cases of infiltration of the muscularis propria, the risk of lymph node metastasis is 25–30% [2], which compromises the curative intent of such deeper resections.

In such cases, total mesorectal excision including regional lymph nodes is preferred. However, this procedure carries major risks, including death (1–3%), ostomy creation, and morbidity [3, 4].

Therefore, the preoperative assessment of infiltration into the muscularis propria (T2 stage) is important. However, there is a lack of reliable diagnostic tools.

F. van den Noort and F. ter Borg share first author position.

✉ F. van den Noort
f.vandennoort@utwente.nl

F. ter Borg
frank2pad@icloud.com

A. Guitink
a.guitink@dz.nl

J. Faber
j.faber@dz.nl

J. M. Wolterink
j.m.wolterink@utwente.nl

[1] Department of Applied Mathematics, Technical Medical Center, University of Twente, Drienerlolaan 5, 7522 NB Enschede, the Netherlands

[2] Department of Gastroenterology & Hepatology, Deventer Hospital, Deventer, the Netherlands

[3] Department of Epidemiology, Deventer Hospital, Deventer, the Netherlands

Published online: 13 December 2024

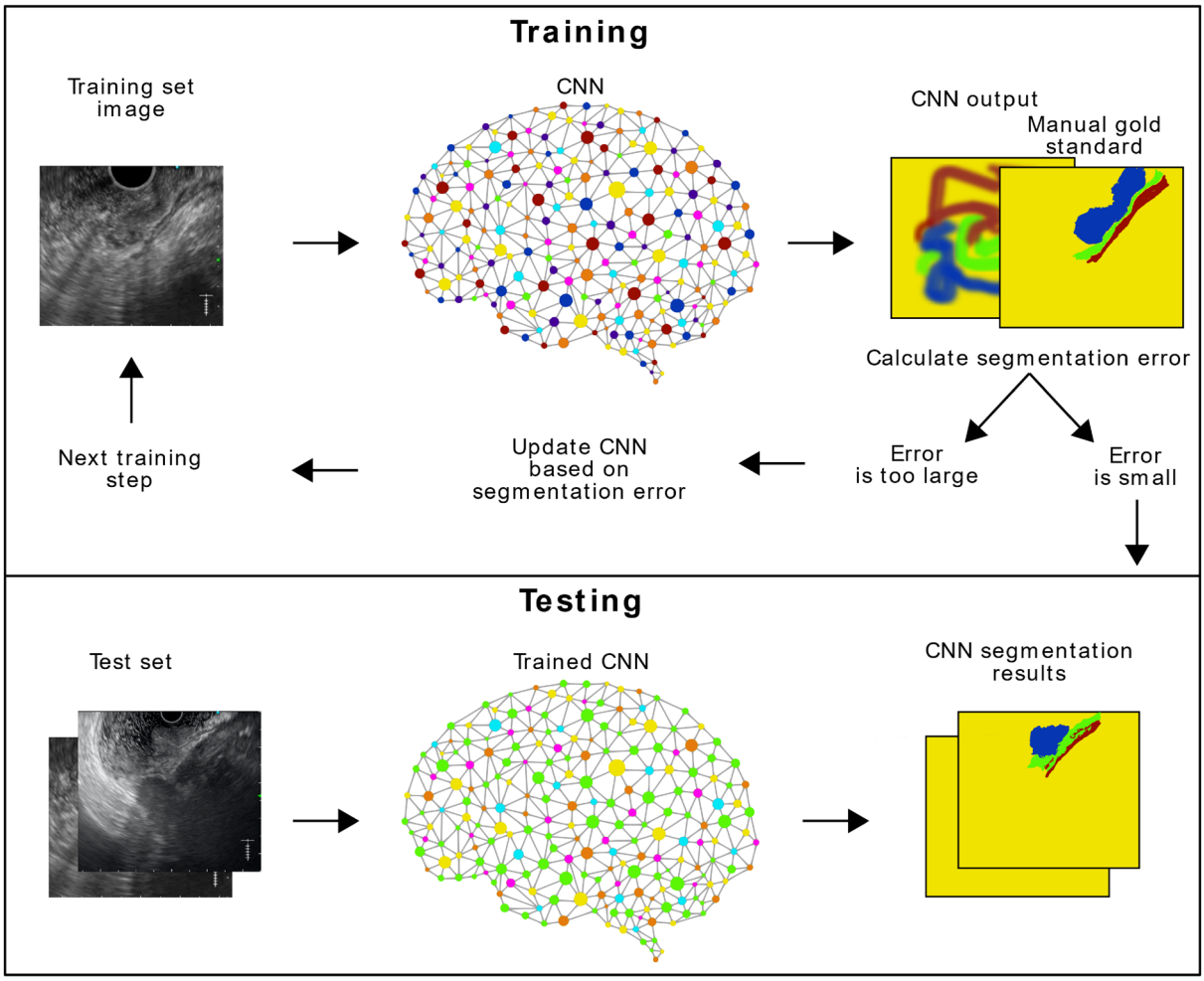

Fig. 1 A visual impression of the learning and testing of a convolutional neural network (CNN). After initializing with random values, training images from the training set are fed into the CNN. The CNN output is compared with the manual gold standard by calculating the error between the two using a loss function. On the basis of this error, the network is updated and the process repeats until the error is small. To check how well the network performs on data not seen before, a test set is kept separate from the training process and used to check the final network performance [20]

Optical characteristics, as obtained by advanced endoscopic imaging, are designed to discriminate between superficial and deep submucosal invasion of the tumor [5] but not the muscularis propria [6, 7]. Some centers consider magnetic resonance imaging (MRI) to be the gold standard for tumor staging, even in cases of early rectal tumor. In addition, the European Society of Gastrointestinal and Abdominal Radiology advises endorectal ultrasound (EUS) for discriminating between cT1 and cT2 stages [8, 9]. The additional use of EUS did not reduce the problem of SPEC overstaging when using MRI alone [10]. Tumor staging can be difficult for both MRI and US, depending on the position, type, and size of the lesion. In addition, both methods depended on the investigator [11].

In the last decade, deep learning, particularly convolutional neural networks (CNN), has become ubiquitous in automated image analysis [12, 13]. Several studies have investigated the use of deep learning for the analysis of endoscopy and EUS, for example, the selection and classification of EUS movie frames [14–16]. Deep learning also has been used to successfully segment bile duct tumors [17]. New advances in US technology with the development of three-dimensional (3D) image acquisition have resulted in a volumetric image that can be saved and analyzed after the acquisition, similar to MRI. Adding deep learning to the analysis will help in many situations. However, it is important to adequately understand how to use deep learning and understand its added value and limitations.

In this study, we investigated the possibility of using deep learning for the segmentation of the (sub)mucosa, muscularis propria, and tumor in EUS images. We hypothesized that successful segmentation of the rectal wall layers and

SPEC using deep learning could be the first step in reducing investigator dependency on EUS.

Patients and methods

General aspects and preparation of images

This was a prospective single-center study. Eighty patients who were referred for the evaluation of rectal SPEC were included. The patients underwent linear EUS (L-EUS) as part of endoscopic assessment. The medical ethics committee of the Isala Clinics (Zwolle, the Netherlands) judged that the study was not subject to the Medical Research Involving Human Subjects Act (WMO), because there was no extra burden to the patient with regards to standard clinical care.

All the patients provided written informed consent for the use of EUS and pathology data. The data were pseudonymized, encrypted, and stored in the Castor Electronic Data Capture System (Castor EDC, version 2022.1, 175 Varick St., Ground Floor, New York, NY 10014, USA) and were accessible only to the investigator.L-EUS was performed with an Olympus GF UCT 180 curvilinear array ultrasound gastrovideoscope using tissue harmonic imaging in resolution mode (THS-R) (Olympus Nederland B.V, Hoofddorp) [18]. This system generates two-dimensional longitudinal images of lesions. Images from the EUS investigations were later analyzed, and a maximum of the five most representative EUS images were selected for manual segmentation (average of 4.66 per patient). These images were chosen to reflect the image variation found during the full examination since manual segmentation of all data obtained during examination is not feasible. The segmentation process was performed by the author (F.t.B.) with 22 years of EUS experience. He developed a segmentation protocol based on the visual recognition of bowel wall layers on EUS images and knowledge of the final pathology of the lesion. This combination of visually available EUS features and pathology was chosen to ascertain the best available delineation of the tumor and bowel wall layers during manual segmentation. Segmentations were performed using 3DSlicer v. 4.11 (National Alliance for Medical Image Computing).

All images were scaled to a 256×256 pixel-scale matrix, and all pixels were normalized to an intensity between 0 and 1.

Convolutional neural network setup

The resulting images were used to train a convolutional neural network (CNN) using the U-net architecture to assign a label (background, lesion/mucosa, submucosa, and muscularis propria) to every pixel [13, 19]. An overview of the training process is shown in Fig. 1 [20].

To increase the variation within the training set, data augmentation was applied using affine transformations that randomly transformed the training data with a 50% chance by applying a rotation between $+0.8$ and -0.8 radians and an image scaling between 0.5 and 1.5. Additionally, in 50% of cases, the images were flipped horizontally.

Cross-validation was performed by dividing the dataset into training, testing, and validation datasets. The CNN was trained 16 times, using cross-validation; each time, 75 patients were used for training (70 patients for training and 5 patients for training validation) and 5 patients as a final test set.

U-nets with different depths, filter sizes, and learning rates were tested. The best-performing network had filter sizes of 32, 64, 128, 256, and 512 for the subsequent U-net

Table 1 Baseline characteristics and their association with T2 + status (chi squared) * Lag time is the time between the date of L-EUS and the date of obtaining definitive pathology

Parameter					*P*-value
Age (years)	Mean: 66.2	SD 7.78	Range 51–85		0.88
Sex	Male: 65%	Female: 35%			0.32
Rectal position	Anterior: 43%	Right: 15%	Left: 22%	Posterior: 16%	0.77
Distance–anus (cm)	Mean: 6.5	SD: 4.76	Range: 0–15		0.84
Lesion size (mm)	Mean: 24.2	SD: 12.6	Range: 10–80		0.77
Paris class	1-sp: 6%	1-s: 79%	IIa: 9%	III: 6%	0.01
Capillary bleeding	Present: 59%	Absent: 41%			0.005
Nongranular part	Present: 78%	Absent: 22%			0.052
Kudo	3s/L: 12%	4: 7%	5i: 26%	5n: 54%	0.003
JNET	2a: 7%	2b: 28%	3: 65%		< 0.0005
Demarcation	Present: 56%	Absent: 44%			0.46
Optical diagnosis	Benign: 16%	T1: 57%	T2: 27%		< 0.0005
Lag time*	Median: 28	IQR: 26	Range 0–78		0.51
Pathology	Benign: 20%	T1: 44%	T2: 26%	T3: 6%	na

Automatic segmentation	Manual segmentation	Original image	Validation parameters
 a.			DT 0.96 DM 0.79 DMP 0.77 HT 5.0 HM 8.9 HMP 5.83 MT 0.97 MM 1.18 MMP 0.93
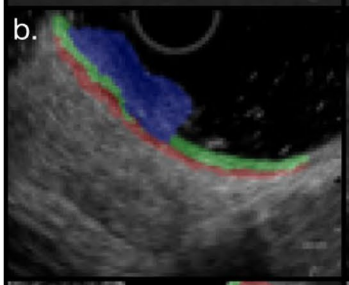 b.	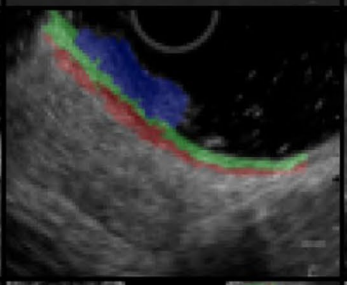		DT 0.82 DM 0.70 DMP 0.70 HT 13.3 HM 13.4 HMP 9.2 MT 3.69 MM 1.90 MMP 1.64
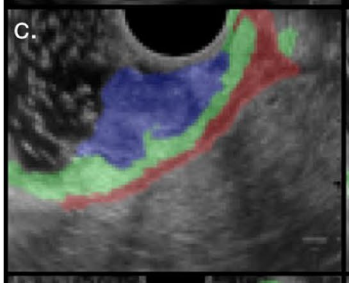 c.			DT 0.70 DM 0.77 DMP 0.88 HT 41.9 HM 24.7 HMP 5.1 MT 10.66 MM 1.70 MMP 0.88
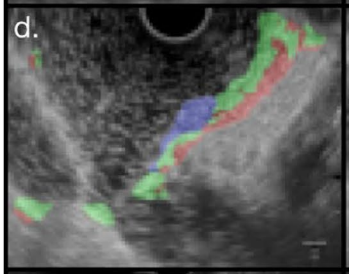 d.	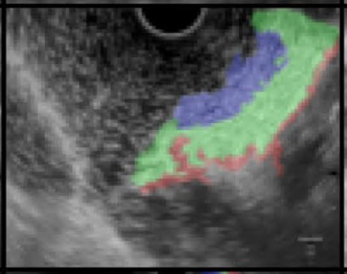	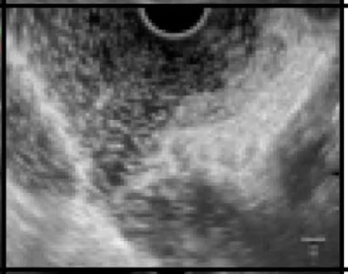	DT 0.33 DM 0.24 DMP 0.12 HT 67.2 HM 40.4 HMP 44.8 MT 10.32 MM 6.75 MMP 22.95
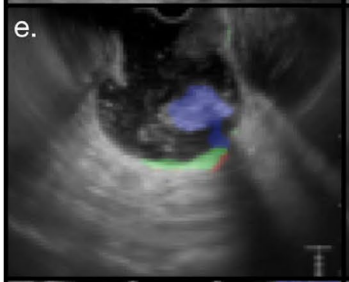 e.	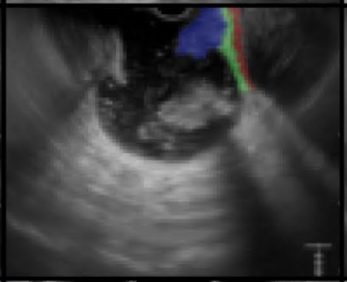		DT 0.00 DM 0.06 DMP 0.00 HT 67.9 HM 30.4 HMP 50.0 MT 44.67 MM 1.43 MMP 10.0
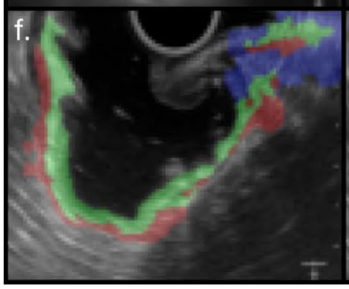 f.	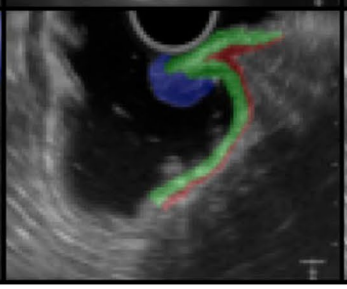		DT 0.00 DM 0.17 DMP 0.13 HT 109.4 HM 59.5 HMP 22.6 MT 59.70 MM 3.21 MMP 0.99

◂**Fig. 2** Six examples (**a–f**) of deep learning segmentations of different quality, with the corresponding manual segmentations and the original image. For each image, the validation parameters are presented in the last column.. These parameters for the tumor (blue), (sub) mucosa (green), and muscularis propria (red) are the Dice similarity index (presented as DT, DM, and DMP, respectively), the Hausdorff distance (HT, HM, and HMP, respectively), and the mean surface distance (MT, MM, and MMP, respectively)

encoding layers. These layers consist of two convolution layers, followed by a max-pooling layer that encodes a part of the network. The decoding part of the network mirrors the encoding layers with a transposed convolution layer, instead of max pooling, to upsample the next layer. Similar to the original U-Net design, the outputs from the encoding layers are also the inputs for their matching decoding layers [21]. The final validation was performed in Python 3.8 using PyTorch 1.9.1 as the deep learning library. The PReLU activation function was used as the activation function using the Pytorch implementation, where α is a learnable parameter [20]. The network was trained using the Adam optimizer ($\beta_1 = 0.9$ and $\beta_2 = 0.99$) with a learning rate of 0.001 and a dropout rate of 0.3 [22].

As a loss function, we used the Dice loss (DL) [23] combined with a cross-entropy loss (CEL), which we masked for an area of 30 pixels around the manually segmented tumor because manual segmentation for (sub)mucsa and muscularis propria was not available for the entire image. The final loss (FL) was calculated as $FL = DL + 0.5CEL$. While optimizing the best network training parameters, this combined loss achieved the best results in discriminating between the submucosa and muscularis propria close to the tumor. U-nets were trained for 2500 epochs with a mini-batch size of 32. The validation loss was checked after every epoch, and the network was saved when the validation loss improved compared with the previous save.

Performance analysis

The CNN segmentations were analyzed by calculating the Dice similarity index (DSI), mean surface distance (MSD), and Hausdorff distance (HDD) between the CNN and manual segmentation, which are commonly accepted mathematical indicators of agreement between segmenations [24]. The DSI is a measure of the overlap between two different segmentations. The MSD and HDD are the mean and maximum distances, respectively, between the borders of the two segmentations. Furthermore, the segmentation quality was subjectively analyzed by an expert (F.t.B.) to judge the clinical usefulness of the segmentations.

Results

Between February 2018 and April 2022, 100 L-EUS procedures were performed for SPEC. In one case, no informed consent was obtained; in six cases, L-EUS media was absent or unreadable; in six cases, the final pathology was unavailable; and in seven cases, primary treatment included (chemo) radiation, rendering pathology irrepresentative.

The final dataset consisted of 80 patients with baseline characteristics (Table 1), and yielded 373 manual segmentations.

Examples of CNN segmentation versus manual segmentation are shown in Fig. 2.

Figure 3 presents box plots of the DSI, MSD, and HDD between the deep learning and manual segmentation of the complete dataset. The DSI values of tumor segmentation (median 0.82) showed excellent agreement between CNN and manual segmentation. The results for the muscularis propria (median 0.59) and submucosa (median 0.57) were less favorable. This can be explained by the fact that the DSI is very sensitive to small shifts between segmentations for small elongated structures. This was confirmed by the fact that the MSD and HDD of the tumor (median of 3.2 and 17.7 pixels, respectively) were similar in the muscularis propria (median 2.6 and 20.0 pixels, respectively) and submucosal (median 3.4 and 24.7 pixels, respectively), respectively. Owing to the different ways in which images are acquired, the resolution can only be estimated from the ruler presented by the ultrasound software on every image and is approximately 0.2 mm per pixel. On average, the distance between the manual and CNN segmentation surfaces was approximately 3 pixels, which translates to an average segmentation error of approximately 0.6 mm. The third quartiles of the MSD were 6.2, 8.1, and 6.5 pixels for the muscularis propria, submucosa, and tumor, respectively, which corresponded to an error of less than 2 mm. A total of 73 CNN segmentations were judged incorrect by the expert, accounting for 19.6% of the total segmented images.

Discussion

To the best of our knowledge, this is the first attempt to develop an automatic segmentation tool that facilitates interpretation of L-EUS media in rectal SPECs.

We showed that the layers of the muscularis propria, submucosa, and tumor, as observed on L-EUS, could be segmented by a CNN, generating useful segmentations in 80.4% of the cases.

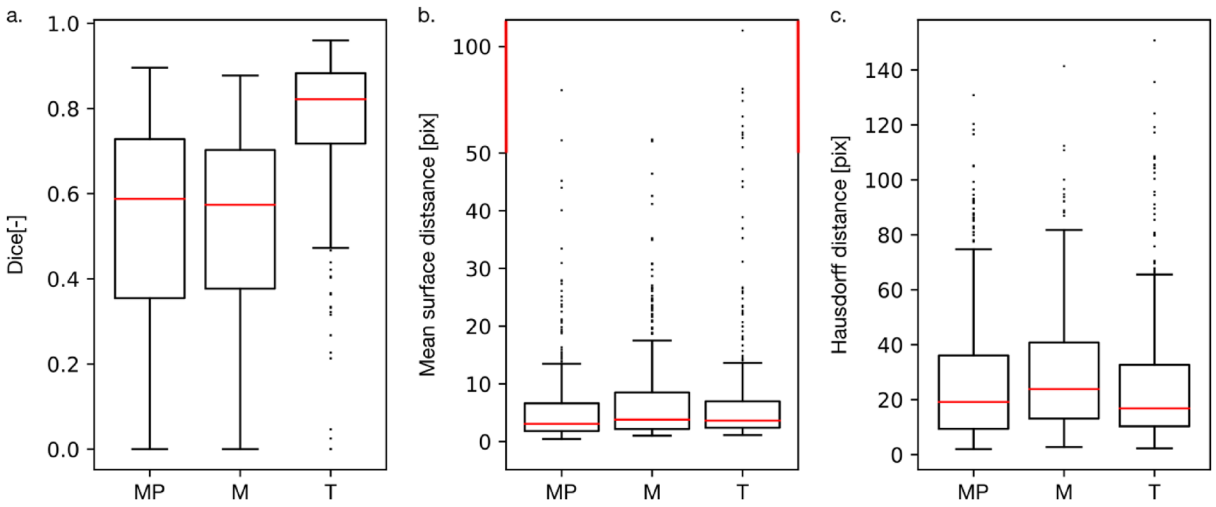

Fig. 3 Box plots of the Dice similarity index (**a**), mean surface distance (**b**) and Hausdorff distance (**c**) between manual and deep learning segmentation of the dataset. Both the mean surface distance and the Hausdorff distance are presented in pixels. The box plots for the tumor(T), (sub)mucosa (M), and muscularis propria (MP) are presented with the median as a red line, boxes that encapsulate the interquartile range (IQR) between the first and third quartile, and whiskers that extend to the full data range, excluding outliers beyond 1.5 times the interquartile range (IQR). To enhance the clarity in **b**, we enlarged the bottom (< 50) part of the graph compared with the top

The quality indicators (DSI, HDD, and MSD) of the CNN are promising, particularly when considering a training set of 373 images from only 80 patients. This problem was effectively addressed using data augmentation. In this way, we obtained comparable CNN performance indicators, as in the larger studies mentioned below.

Isawa et al. trained a CNN on the data of 100 patients (900 images per patient) to segment pancreatic tumors using contrast-enhanced EUS images [24]. They reported a median intersection over union (IoU) of 0.77. As the IoU is slightly more penalizing than the DSI, this finding is comparable to our median of 0.82 DSI.

Li et al. trained a CNN for gastrointestinal stromal tumor segmentation using 905 patients (1805 images) for training and testing [25]. Their CNN achieved a mean DSI of 0.92, a mean HDD of 11.72 pixels, and a mean MSD of 3.14 pixels. The DSI and HDD were slightly better than our results, but the MSD values were comparable. They also trained a standard U-net for this task, which performed considerably worse (DSI of 0.71, HDD of 37.4 pixels, and MSD of 13.8 pixels).

Zhang et al. automatically segmented the pancreas and blood vessels by using EUS images. The DSI was 0.77 for the pancreas [26]. Yao et al. performed bile duct segmentation and reported a DSI of 0.72 [27]. It is difficult to compare these results with our study because no MSD and HDD were reported, and the appearance of these structures greatly influences the DSI and cannot be easily estimated from these works. However, these DSI scores were either comparable to or lower than our tumor segmentation results, and better than our submucosal and muscularis propria results.

The clinical applicability of these results still has a way to go; however, on the basis of this study, the CNN platform can be further extended by training with a larger training set to make it more generalizable to the complete patient population and image acquisition variation (tumor sizes, ultrasound artifacts, etc.). This will eventually result in a system that can generate segmented EUS images in real time that could be used in three-dimensional reconstructions, but this needs to be incorporated into the commercial software packages of ultrasound machines so it can be used by other clinicians. In this way, the main limitation of EUS, namely investigator dependence, may be reduced, and the interpretation of images be facilitated, likely reducing the training time to learn to operate EUS. We do not believe that CNN will make a final diagnosis of the T-stage in the near future, but it will function as a major help in the interpretation of EUS, as is the case with other CNN systems, such as polyp recognition. This may also facilitate EUS training in rectal SPECs.

Our study has several strengths. We achieved our segmentation results for a large variety of image qualities and appearances, such as different tumor sizes and bowel folds. We did not select images, and low-quality images were used. The data were obtained directly from clinical practice, thus providing a good representation of the clinical reality.

Our study has some limitations. Training data were obtained using one type of EUS probe, and manual segmentation was performed by a single observer (F.t.B.). This limits the generalizability of our algorithm to other ultrasound systems and introduces a bias toward the segmentation style of this single observer. However, in a pilot study, this was inevitable, and

manual segmentation was performed to fit the data obtained during the pathological examination, thus minimizing personal influence.

Conclusions

Our results show that automatic segmentation of EUS is feasible and therefore encourages further exploration of CNN-based EUS segmentation for rectal SPEC, facilitating interpretation and diminishing interobserver variation.

Acknowledgements This study was financially supported by an unrestricted research grant from the Pioneers in Health Care Innovation Fund, established by the University of Twente, Saxion University of Applied Sciences, Medisch Spectrum Twente, Ziekenhuis Groep Twente, Deventer Hospital, and Reggeborgh BV.

Author contributions F.v.d.N., F.t.B., and J.M.W. developed the study design. F.N. and J.M.W. were involved in network training and testing. F.t.B. provided manual segmentation and clinical validation of the data. A.G. and J.F. were involved in patient management and patient inclusion. All authors reviewed the manuscript.

Funding This study was funded by the Pioneers in Healthcare fund. Study name: Artificial inTelligence-empowered endo-ultrasonographic assessment of bowel wall infiltration in early colorectal cancer (a Tempo study).

Data availability No datasets were generated or analyzed during the current study.

Declarations

Conflict of interest The authors declare no competing interests.

Patient consent statement All the patients provided written informed consent for the use of EUS and pathology data.

Clinical trail registration The medical ethics committee of the Isala Clinics (Zwolle, Netherlands) judged that the study was not subject to the Medical Research Involving Human Subjects Act (WMO), because there was no extra burden to the patient with regards to standard clinical care.

Ethical approval In the methods we state the following: The medical ethics committee of the Isala Clinics (Zwolle, the Netherlands) judged that the study was not subject to the Medical Research Involving Human Subjects Act (WMO), because there was no extra burden to the patient with regards to standard clinical care.

Informed consent This means that the medical ethics commitee checked the study but judged that no ethical approval was needed, only informed consent of the patients to use their data in the study. This was decided since there is no extra burden to the patients. The data was already collected as part of their path to correct polyp diagnosis.

References

1. Toes-Zoutendijk E, van Leerdam ME, Dekker E, van Hees F, Penning C, Nagtegaal I, van der Meulen MP, van Vuuren AJ, Kuipers EJ, Bonfrer JMG, Biermann K, Thomeer MGJ, van Veldhuizen H, Kroep S, van Ballegooijen M, Meijer GA, de Koning HJ, Spaander MCW, Lansdorp-Vogelaar I, Dutch National Colorectal Cancer Screening Working Group (2017) Real-time monitoring of results during first year of dutch colorectal cancer screening program and optimization by altering fecal immunochemical test cut-off levels. Gastroenterology 152:767–775
2. Ushigome H, Ohue M, Kitamura M, Nakatsuka S, Haraguchi N, Nishimura J, Yasui M, Wada H, Takahashi H, Omori T, Miyata H, Yano M, Takiguchi S (2020) Evaluation of risk factors for lymph node metastasis in T2 lower rectal cancer to perform chemoradiotherapy after local resection. Mol Clin Oncol 12:390–394
3. Vermeer NCA, Backes Y, Snijders HS, Bastiaannet E, Liefers GJ, Moons LMG, van de Velde CJH, Peeters KCMJ (2018) Dutch T1 Colorectal Cancer Working Group National cohort study on postoperative risks after surgery for submucosal invasive colorectal cancer. BJS Open. 3(2):210–217. https://doi.org/10.1002/bjs5.50125. (**PMID: 30957069; PMCID: PMC6433330**)
4. Vermeer NCA, Backes Y, Snijders HS et al (2019) National cohort study on postoperative risks after surgery for submucosal invasive colorectal cancer. BJS Open 3:210–217
5. Tanaka S, Saitoh Y, Matsuda T, Igarashi M, Matsumoto T, Iwao Y, Suzuki Y, Nozaki R, Sugai T, Oka S, Itabashi M, Sugihara KI, Tsuruta O, Hirata I, Nishida H, Miwa H, Enomoto N, Shimosegawa T, Koike K (2021) Evidence-based clinical practice guidelines for management of colorectal polyps. J Gastroenterol. https://doi.org/10.1007/s00535-021-01776-1. (**Epub ahead of print. PMID: 33710392**)
6. Mori Y, Kudo SE, Endo S, Maeda C, Mukai S, Maeda Y, Kataoka S, Takeda K, Ichimasa K, Miyachi H, Sawada N, Hidaka E, Ishida F (2016) Morphology as a risk factor for the malignant potential of T2 colorectal cancer. Mol Clin Oncol 5(3):223–226
7. Koyama Y, Yamada M, Makiguchi ME, Sekiguchi M, Takamaru H, Sakamoto T, Kono S, Fukuzawa M, Sylvia Wu SY, Sugumaran A, Kawai T, Matsuda T, Itoi T, Saito Y (2022) New scoring system to distinguish deep invasive submucosal and muscularis propria colorectal cancer during colonoscopy: a development and global multicenter external validation study (e-T2 Score). Gastrointest Endosc 8:S0016-5107
8. Please refer to: https://richtlijnendatabase.nl/richtlijn and colorectal carcinoma and diagnostics, 2019. Accesed 20 Nov 2024.
9. Beets-Tan RGH, Lambregts DMJ, Maas M, Bipat S, Barbaro B, Curvo-Semedo L et al (2018) Magnetic resonance imaging for clinical management of rectal cancer: updated recommendations from the 2016 European Society of Gastrointestinal and Abdominal Radiology (ESGAR) consensus meeting. Eur Radiol 28:1465–1475
10. Detering R, van Oostendorp SE, Meyer VM, van Dieren S, Bos ACRK, Dekker JWT, Reerink O, van Waesberghe JHTM, Marijnen CAM, Moons LMG, Beets-Tan RGH, Hompes R, van Westreenen HL, Tanis PJ, Tuynman JB (2020) on behalf of the Dutch ColoRectal Audit Group: MRIcT1–2 rectal cancer staging accuracy: a population-based study. BJS 107:1372–1382
11. El Hajj II, DeWitt J, Sherman S, Imperiale TF, LeBlanc JK, McHenry L, Cote GA, Johnson CS, Al-Haddad M (2018) Prospective evaluation of the performance and interobserver variation in endoscopic ultrasound staging of rectal cancer. Eur J Gastroenterol Hepatol 30:1013–1018
12. Krizhevsky A, Sutskever I, Hinton GE. 2012 ImageNet Classification with Deep Convolutional Neural Networks. Proc 25th Int Conf Neural Inf Process Syst 1:1097–105.

13. Litjens G, Kooi T, Bejnordi BE, Arindra A, Setio A, Ciompi F et al (2017) A survey on deep learning in medical image analysis. Med Image Anal 42:60–88
14. Cai YW, Dong FF, Shi YH, Lu LY, Chen C, Lin P et al (2021) Deep learning driven colorectal lesion detection in gastrointestinal endoscopic and pathological imaging. World J Clin Cases 9:9376–9385
15. Kuwahara T, Hara K, Mizuno N, Haba S, Okuno N, Koda H et al (2021) Current status of artificial intelligence analysis for endoscopic ultrasonography. Dig Endosc 33:298–305
16. Tonozuka R, Mukai S, Itoi T (2021) The role of artificial intelligence in endoscopic ultrasound for pancreatic disorders. Diagnostics 11:18
17. Yao L, Zhang J, Liu J, Zhu L, Ding X, Chen D et al (2021) A deep learning-based system for bile duct annotation and station recognition in linear endoscopic ultrasound. EBioMedicine. https://doi.org/10.1016/j.ebiom.2021.103238
18. Matsumoto K, Katanuma A, Maguchi H, Takahashi K, Osanai M, Yane K, Kin T, Takaki R, Matsumori T, Gon K, Tomonari A, Nojima M (2016) Performance of novel tissue harmonic echo imaging using endoscopic ultrasound for pancreatic diseases. Endosc Int Open 4(1):E42-50
19. Ronneberger O, Fischer P, Brox T. U-Net: Convolutional Networks for Biomedical Image Segmentation. Int Conf Med image Comput Comput Interv. 2015;234–41.
20. van den Noort F, van der Vaart CH, Grob ATM, van de Waarsenburg MK, Slump CH, Van Stralen M (2019) Deep learning enables automatic quantitative assessment of puborectalis muscle and urogenital hiatus in plane of minimal hiatal dimensions. Ultrasound Obstet Gynecol 54:270–275
21. Ushigome H, Ohue M, Kitamura M, Nakatsuka S, Haraguchi N, Nishimura J, Yasui M, Wada H, Takahashi H, Omori T, Miyata H, Yano M, Takiguchi S (2020) Evaluation of risk factors for lymph node metastasis in T2 lower rectal cancer to perform. Mol Clin Oncol 3;12(4):390–394
22. He K, Zhang X, Ren S, Sun J 2015 Delving Deep into Rectifiers: Surpassing Human-Level Performance on ImageNet Classification. arXiv Prepr arXiv150201852
23. Kingma DP, Ba JL. Adam 2015 A method for stochastic optimization. In: 3rd International Conference on Learning Representations, ICLR 2015—Conference Track Proceedings. International Conference on Learning Representations, ICLR
24. Iwasa Y, Iwashita T, Takeuchi Y, Ichikawa H, Mita N, Uemura S et al (2021) Automatic segmentation of pancreatic tumors using deep learning on a video image of contrast-enhanced endoscopic ultrasound. J Clin Med 10:3589
25. Li X, Guo Y, Jiang F, Xu L, Shen F, Jin Z et al (2020) Multi-task refined boundary-supervision U-Net (MRBSU-Net) for gastrointestinal stromal tumor segmentation in endoscopic ultrasound (EUS) Images. IEEE Access 8:5805–5816
26. Zhang J, Zhu L, Yao L, Ding X, Chen D, Wu H et al (2020) Deep learning–based pancreas segmentation and station recognition system in EUS: development and validation of a useful training tool. Gastrointest Endosc 92:874-885.e3
27. Yao L, Zhang J, Liu J, Zhu L, Ding X, Chen D, Wu H, Lu Z, Zhou W, Zhang L, Xu B, Hu S, Zheng B, Yang Y, Yu H (2021) A deep learning-based system for bile duct annotation and station recognition in linear endoscopic ultrasound. EBioMedicine. https://doi.org/10.1016/j.ebiom.2021.103238